Juni Khyat
(UGC Care Group I Listed Journal)
ISSN: 2278-4632
Vol-13 Issue-01 2023

Analyzing Breast Cancer Images Histopathologically using Deep Learning

Mrs. K. RAMA LAKSHMI[1], Mr. INDRAGANTI VENKATA RAVI KUMAR[2], Mrs. V. LAVANYA[3]
ASSISTANT PROFESSOR[1,3] ,ASSOC PROFESSOR[2]
DEPARTMENT OF ECE, SWARNANDHRA COLLEGE OF ENGINEERING AND TECHNOLOGY, NARASAPUR

Abstract

A major issue in public health, breast cancer ranks first in terms of morbidity rates among cancer types. A patient's prognosis improves considerably and many potentially fatal disorders are curable if detected early. Nevertheless, this process requires the knowledge and experience of pathologists and may be somewhat laborious. The clinical and prognosis consequences of automatically identifying breast cancer by histological image analysis are significant. Nevertheless, traditional feature extraction methods are limited to extracting just a handful of surface-level attributes from images; hence, selecting pertinent qualities requires specialized knowledge. Using deep learning algorithms, it is possible to automatically extract high-level abstract features from pictures. Consequently, we use it to analyze breast cancer histopathology photographs using supervised and unsupervised deep convolutional neural networks. We started by adapting the Inception ResNet V2 and Inception V3 architectures using transfer learning so they could tackle the binary and multi-class challenges of breast cancer histopathology picture categorization. After that, the histological images were rotated 90 degrees and 180 degrees counterclockwise to eliminate any bias that may have been generated by the unequal distribution of the photos, and the subclasses were rebalanced using Ductal Carcinoma as the baseline. The histological picture classification of breast cancer using Inception V3 and Inception ResNet V2 is obviously the best alternative available at the moment, when compared to earlier methodologies and our own experimental results.

Keywords:

images of breast cancer tissue samples for the purpose of diagnosis; autoencoder; transfer learning; classification; clustering; deep convolutional neural networks).

INTRODUCTION

Cancer is one of the top public health concerns of our day. Worldwide, the number of cancer diagnoses increased by 28% from 2006 to 2016, and by 2030, the International Agency for Research on Cancer (IARC) of the World Health Organization and the Global Burden of Disease Cancer Collaboration predict that an additional 2.7 million cases will be reported (Boyle and Levin, 2008; Moraga-Serrano, 2018). With almost 1.5 million new cases, 535,000 fatalities, and 14.9 million disability-adjusted life years (DALYs) in 2018, breast cancer is a leading cause of cancer-related deaths among women. Consequently, early detection of breast cancer is of the utmost importance. Biopsy procedures are still the main methods relied on for accurate breast cancer diagnosis, despite the 40 years of usage of imaging techniques such as X-ray, MRI, ultrasound, etc. (Stenchiest et al., 1978). The most frequent ways for performing a biopsy are surgical biopsy, vacuum-assisted biopsy, and fine-needle aspiration. Cells and tissues are prepared for microscopic analysis by collecting, fixing, and staining samples (Vita et al., 2014). Spanhol et al. (2016a) state that pathologists use histological images to arrive at a diagnosis. Analyzing histopathological images is a laborious and intricate procedure that requires knowledge from specialists. Results may also vary depending on the level of experience of the pathologists that took part in the research. Consequently, computer-aided interpretation of histological images is crucial for the diagnosis and prognosis of breast cancer (Aswathy and Jagannath, 2017). However, the following challenges hinder the development of tools for doing this study. Detailed, high-resolution images brimming with intriguing patterns and forms are what breast cancer histopathology photographs are all about. Due to both intra- and inter-class variation, categorization may be particularly difficult when working with many classes. The second issue is the limitations of the present feature extraction methods when it comes to breast cancer histopathology images. Current feature extraction methods rely on supervised data. For example, SIFT (Lowe, 1999) and GLCM (Hara lick et al., 1973) are examples of such methods. Since it need prior knowledge of the data to discern significant features, the computational overhead is enormous, and the feature extraction efficacy is low. The last features that were extracted are low-level, rather irrelevant properties of histopathology images. The final resultant model can therefore fail to adequately perform the classification job for which it was designed.

Related Texts

ISSN: 2278-4632
Vol-13 Issue-01 2023

Over the last four decades, researchers have made great strides in improving image-based breast cancer diagnosis. One school of thought may use more traditional machine learning methods, while the other could lean more toward deep learning. Because of their familiarity with small datasets of breast cancer images, the first group often uses laborious and wasteful abstract features. The second set can process massive amounts of data and automatically pull out even more nebulous features. For example, in 2012, Zhang et al. (2013) presented a new cascade random subspace ensemble method with rejection choices for microscopic biopsy picture classification. Two sets of random subspace classifiers are used in this classification technique. The first ensemble consists of a set of support vector machines trained on a series of K binary classification problems generated from the original K-class classification problem (K = 3). Another ensemble, this one using Multi-Layer Perceptrons, looks at the previous ensemble's rejected samples. Of the 361 images used to assess the system, 119 depicted healthy tissue, 102 showed cancer cells in situ, and 140 showed either lobular carcinoma or invasive ductal carcinoma. A random sample of 20% of each class's pictures was used for testing, while the remaining images were used for instruction. Classification accuracy was 99.25%, reliability was 97.50%, and rejection was 1.94%. Using four distinct clustering methods, Kowal et al. (2013) successfully segmented 500 images from fifty breast cancer patients. Next, three separate classification algorithms were used to the images, with the goal of distinguishing between benign and malignant tumors. Fifty healthy cases and fifty cancer cases were represented by ten images each, for a grand total of five hundred photographs.

They achieved a classification accuracy of 96% to 100% by using 50-fold cross-validation. Flick et al. (2013) introduced a method for the diagnosis of breast cancer by analyzing cytological images of small needle biopsies. We utilized four classic machine learning techniques—KNN (K nearest neighbour with K = 5), DT (decision tree), and SVM (support vector machine with Gaussian radial basis function kernel and scaling factor = 0.9)—along with twenty-five nuclei features to build classifiers for the biopsies. To test these classifiers, we employed a dataset consisting of 737 microscopic photos of tiny needle biopsies collected from 67 people; the dataset includes 42 instances of cancer (462 images) and 25 cases of benign (275 images). The maximum efficiency that has been reported is 98.51%. A method for the diagnosis of breast cancer was proposed by George et al. (2014) using nuclear segmentation from cytological images. The classification models used were SVM, PNN, LVQ, and MLP, which stands for multilayer perceptron utilizing the backpropagation approach. Table 5 from George et al. (2014) provides information on the model parameters. Using 10-fold cross validation, a classification accuracy of 76-44% may be achieved with only 92 pictures, 45 of which show benign tumors and 47 of which show malignant tumors. Using the 699-sample Wisconsin Breast Cancer dataset (458 benign and 241 malignant cases), Asri et al. (2016) assessed the efficacy of four ML algorithms: SVM, DT, NB, and KNN. The experimental findings shown that SVM with 10-fold cross-validation achieved the highest degree of accuracy (97.13%).

Procedures and Information Gathering

The BreaKHis dataset used in this study was given by Spanhol et al. (2016a). There are a total of 82 breast cancer patients that were seen in the clinic, with 7,909 histological photos included. Visit http:// web.inf.ufpr.br/vri/breast-cancer-database to access the database. The pathologist took each image by preserving the original structural and molecular composition of the breast tissue sample taken after surgery. To produce the final images, haematoxylin and eosin stains were used. Pathologists finally determined the proper categorization of each image based on their examinations under the microscope. These three-channel RGB micrographs (700 460 in total) are used for all breast cancer histology photos. Since different objective lenses were used to capture these breast cancer histology images, the whole dataset was split into four groups: 40X, 100X, 200X, and 400X.

The benign or malignant status of the tumors in question is used to classify these supplemental datasets. As a result, two kinds of tumors are considered benign, while the other two are classified as malignant. Benign tumors (TA) include adenosis (A), fibroids (F), phyllodes tumors (PT), and tubular adenomas (T). Cancers that are malignant include lobular, dactylous, papillary, and ductal carcinomas. The example descriptions of the Break His dataset are presented in Table 1. To fit the required input size of the network structure—299 299 for both the Inception V3 and Inception ResNet V2 networks used in this article—all of the breast cancer histopathology photographs must be transformed into 299 299 images. The transformation procedure made use of TensorFlow's image preparation capabilities, which included cutting the border box, resizing, and changing the saturation. Consequently, the model's input size was accurately reflected in the resulting three-channel image, which had pixel values normalized to the range [1, 1]. To ensure that the experimental results in the classification task could be applied to other situations, the datasets for the four magnification factors were split into training and testing subsets at random at a ratio of 7:3.

Data Organization Framework

ISSN: 2278-4632
Vol-13 Issue-01 2023

Here we will discuss our expertise in classifying breast cancer histopathology images using the Inception ResNet V2 (Szeged et al., 2017) and Inception V3 (Szeged et al., 2016) deep learning models, along with our analysis of the results.

Interconnections and Networks for Classification

The networks used in our experiments are Inception ResNet V2 (Szeged et al., 2017) and Inception V3 (Szeged et al., 2016), which were proposed by the same authors in 2016 and 2017, respectively. It was shown in the ILSVRC competition that, when trained on big datasets, the Inception ResNet V2 network may surpass the Inception V3 network. A key difference between the Inception V3 and Inception ResNet V2 networks is the existence of residual connections in the latter. Using histopathology images of breast cancer as input, we compare the experimental results obtained from Inception ResNet V2 and Inception V3 on small datasets to determine which network performs better. These network diagrams are shown in Figure 1. Figure 1 shows that the two networks are structurally comparable. A stack of Inception modules forms the core, while traditional convolutional and pooling layers execute a characteristic transformation in the first few layers. Finally, the fully-connected layer is utilized to output the findings by using the SoftMax function. Both the Inception ResNet V2 and Inception V3 networks' Inception modules are essentially distinct from one another. To make the Inception V3 network more adaptable to different convolution kernels, its modules include filters of different sizes, such as1,1,3, and 3 1. To avoid the common problem of a network gradient degrading as the number of layers increases, the Inception ResNet V2 network incorporates a residual unit into every Inception module. Various filters are also available.

TABLE 1 | Image distribution of different subclasses in different magnification factors

Magnification	Benign				Malignant				Total
	A	F	PT	TA	DC	LC	MC	PC	
40X	114	253	109	149	864	156	205	145	1,995
100X	113	260	121	150	903	170	222	142	2,081
200X	111	264	108	140	896	163	196	135	2,013
400X	106	237	115	130	788	137	169	138	1,820
Total	444	1,014	453	569	3,451	626	792	560	7,909
#Patients	4	10	3	7	38	5	9	6	82

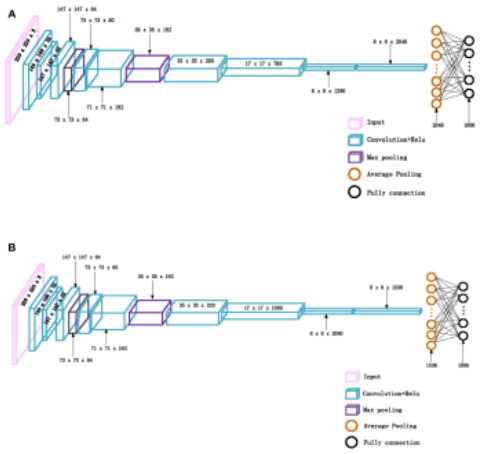

FIGURE 1 The network structures, (A) Inception_V3, (B) Inception_ResNet_V2

With residual connections, layer-jumping becomes feasible at higher network sizes, reducing the impact of node density. Figure 2 shows a comparison between Inception ResNet V2 and the 8x8 Inception modules seen in Inception V3. Szeged et al. (2016) and (2017) provide more information.

Skill Transfer

ISSN: 2278-4632
Vol-13 Issue-01 2023

According to Pan and Yang (2010), one significant use of deep learning is transfer learning. Anyone can tell you that a little dataset isn't going to be enough to train a complex deep network. Furthermore, no set criteria exist for designing a network architecture to achieve a certain objective. Rather of starting from scratch, we may use the collected data as a foundation for our own study by including the model and parameters found from previous studies that used the computationally expensive and time-consuming ImageNet dataset. After that, we may retrain the model with a little amount of data and still get good results on our target task using the final defined fully-connected layer.

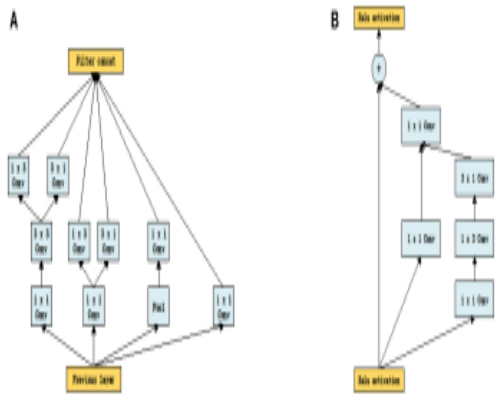

FIGURE 2 | The inception module of size 8 × 8 in two networks, (A) Inception_V3, (B) Inception_ResNet_V2

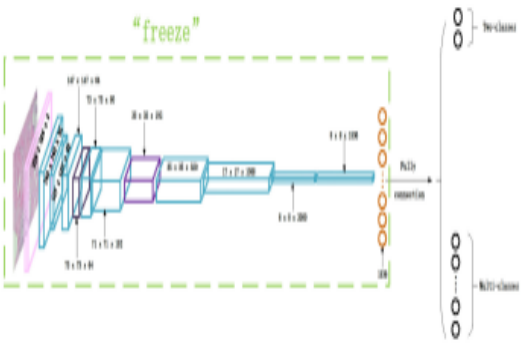

FIGURE 3 | The Inception_ResNet_V2 network structure for transfer learning.

The histological pictures of breast cancer are classified using Inception_V3 and Inception_ResNet_V2 networks via the use of transfer learning in this research. We started by getting the Inception ResNet V2 and Inception V3 models and parameters from the ImageNet dataset. About 1.2 million photos are used for training, 50,000 for validation, and 100,000 for testing. There are a grand total of 1,000 distinct types included in this. After that, we stopped adjusting any of the settings up to the very last network layer. For binary classification, we adjusted the final fully-connected layer's neuron count to 2, and for multi-class classification, we increased it to 8. Afterwards, breast cancer histopathology photos are used to train the parameters of the fully-connected layer. The Inception ResNet V2 network's updated architecture is seen in Figure 3. Because it is so similar, we will not be discussing the updated Inception V3 network architecture. On top of the TensorFlow deep learning framework, we built our categorization method. During training, the Adam algorithm was used to optimize the model using a dataset of breast cancer histopathology images. The method was designed by Kingman and Ba (2014) and iteratively ran through 70 epochs. In the studies, Bergstrom and Bagnio (2012) set the batch size to 32 and the starting learning rate at 0.0002. Then, to make sure the model goes through its initial training iterations fast and minimize the learning rate, the exponential decay approach is used. Additionally, this facilitates the acquisition of the ideal solution and aids in providing greater stability in the subsequent stages. According to Bergstrom and Bagnio (2012), the decay coefficient is set at 0.7, and the decay speed is adjusted so that it happens every two epochs. In (1), we can see the concrete decay process, with the variables decayed_learning_rate, learning rate, decahydrate, global step, and decay stages representing the many variables.

ISSN: 2278-4632
Vol-13 Issue-01 2023

$$decayed\_learning\_rate = learning\_rate \times decay\_rate^{(global\_step/decay\_steps)} \quad (1)$$

Results of Climatic Grouping

Here we will discuss the time-saving ability of the Inception ResNet V2 network to automatically extract meaningful features from breast cancer histopathology photos. Using Inception ResNet V2, features are extracted along 1,536 dimensions in histopathological breast cancer photos. The K-means approach is then used for clustering. For the purpose of applying a non-linear adjustment to the 1,536-dimensional feature vectors generated by Inception ResNet V2, a new AE (Autoencoder) network is constructed with dimensions [1536, 500, 2]. The two-dimensional features of breast cancer histology images may be extracted in this way, and K-means can use them. Our suggested AE uses features obtained by Inception ResNet V2 to modify features, and the combined effect is IRV2+Kmeans, which represents clustering results from K-means utilizing Inception ResNet V2 features.

TABLE 3 Paired rank comparison of algorithms in ACC_IL and AII_PL for binary and multi-class classification

ACC_IL for binary	IRV2_Aug	IRV2_Raw	INV3_Raw	CSDCNN_Raw(29)	AlexNet_Raw(25)
IRV2_Aug		1.25	2.75	2.0	4.0
IRV2_Raw			1.5	0.75	2.75
INV3_Raw				−0.75	1.25
CSDCNN_Raw(29)					2.0
AlexNet_Raw(25)	*				

ACC_PL for binary	IRV2 _Aug	IRV2 _Raw	INV3 _Raw	CSDCNN _Raw(29)	AlexNet _Raw(25)	PFTAS+SVM _Raw(5)	PFTAS+QDA _Raw(5)
IRV2_Aug		2.75	2.0	2.0	4.0	5.0	5.25
IRV2_Raw			−0.75	−0.75	1.25	2.25	2.5
INV3_Raw				0.0	2.0	3.0	3.25
CSDCNN_Raw(29)					2.0	3.0	3.25
AlexNet_Raw(25)						1.0	1.25
PFTAS+SVM_Raw(5)	*						0.25
PFTAS+QDA_Raw(5)	*						

ACC_IL for multi-class	IRV2 _Aug	IRV2 _Raw	INV3 _Raw	CSDCNN _Aug(29)	CSDCNN _Raw(29)	AlexNet _Aug(29)	AlexNet _Raw(29)	LetNet _Aug(29)	LeNet _Raw(29)
IRV2_Aug		3.0	4.0	1.0	2.5	4.5	6.0	7.0	8.0
IRV2_Raw			1.0	−2.0	−0.5	1.5	3.0	4.0	5.0
INV3_Raw				−3.0	−1.5	0.5	2.0	3.0	4.0
CSDCNN_Aug(29)					1.5	3.5	5.0	6.0	7.0
CSDCNN_Raw(29)						2.0	3.5	4.5	5.5
AlexNet_Aug(29)							1.5	2.5	3.5
AlexNet_Raw(29)								1.0	2.0
LeNet_Aug(29)	*								1.0
LeNet_Raw(29)	*								

ACC_PL for multi-class	IRV2 _Aug	IRV2 _Raw	INV3 _Raw	CSDCNN _Aug(29)	CSDCNN _Raw(29)	AlexNet _Aug(29)	AlexNet _Raw(29)	LetNet _Aug(29)	LeNet _Raw(29)
IRV2_Aug		3.75	3.0	1.0	2.5	4.75	6.0	7.0	8.0
IRV2_Raw			−0.75	−2.75	−1.25	1.0	2.25	3.25	4.25
INV3_Raw				−2.0	−0.5	1.75	3.0	4.0	5.0
CSDCNN_Aug(29)					1.5	3.75	5.0	6.0	7.0
CSDCNN_Raw(29)						2.25	3.5	4.5	5.5
AlexNet_Aug(29)							1.25	2.25	3.25
AlexNet_Raw(29)								1.0	2.0
LeNet_Aug(29)	*								1.0
LeNet_Raw(29)	*								

[†]The upper triangle shows the difference between algorithms. The lower triangle shows pairs with statistical significance. Asterisks indicate significant difference between the pairs of algorithms in the table.

extent to which components are separated and condensed; useful even in the absence of mark data. One to one is the range of SSE. Higher SSE values suggest that the samples are more densely packed, whereas lower values imply that the samples are more widely spread from different groups. Grouping becomes more pronounced when the SSE values approach 1.

Evaluating Results

Here we will compare the clustering results of IRV2+AE+Kmeans with IRV2+Kmeans using external metrics including ACC, ARI, and AMI, as well as the internal metric SSE. Figure 7 displays clustering results for datasets of different magnifications according to the four criteria discussed earlier. The following is shown by the experimental results in Figure 7. (1) IRV2+AE+Kmeans outperforms IRV2+Kmeans in clustering on all datasets and scaling factors with respect to ARI, AMI, SSE, and ACC. The Inception ResNet V2 network can extract features, but our proposed AE network can encode them to provide features that are far more abstract and expressive. For the same clustering, the values of ARI, AMI, SSE, and ACC are growing even without making any changes to the features created by Inception ResNet V2. Finally, the best clustering accuracy (ACC) on the 200X dataset is 76.4% when using features converted by the proposed AE network using extracted features from the Inception ResNet V2 network, whereas on the 40X dataset the highest ACC is 59.3% when using features generated by the Inception ResNet V2 network. Finally, IRV2+Kmeans has a top ACC of 59.3%, whereas IRV2+AE+Kmeans has a superior ACC of 76.4%.

Conclusion

ISSN: 2278-4632
Vol-13 Issue-01 2023

Our methods for analyzing breast cancer histopathology images using Inception ResNet V2 and Inception V3, two deep convolutional neural networks trained utilizing transfer learning techniques, were detailed in this article. The enormous image database ImageNet has already been used to train these two networks. Once they've learned the structure and settings, they're set in stone. To make the fully-connected layer work best for our task, we retrained its settings and tweaked its neuron count. This makes the model suitable for binary or multi-class classification of breast cancer histopathology images. We demonstrate that the Inception ResNet V2 network outperforms the Inception V3 network in analyzing breast cancer histopathology photographs by comparing our experimental results to those of prior studies.

Using the enhanced datasets also significantly improves our experimental results compared to the original datasets. This is especially the case when we use our breast cancer histology images for multi-class classification. When we compare the experimental results of the networks we used as references with those of the Inception ResNet V2 network, we see that it extracts much more informative features. An analysis of breast cancer histopathology photographs using the popular clustering approach K-means revealed that the intrinsic criteria of SSE might be utilized to identify the appropriate K-means value. The proposed AE network has the potential to detect much more useful, low-dimensional features in breast cancer histopathology images.

REFERENCES

[1]In 2017, a group of researchers including Araújo, Arista, Castro, Rouco, Aguiar, Eloy, and others published a paper. Image classification based on breast cancer histology using CNNs. DOI: 10.1371/journal.pone.0177544 PLoS ONE 12:e0177544.

[2] in With contributions by Mousannif, Al Moatassime, Noel, and Asri (2016). Breast cancer risk prediction and diagnosis using machine learning algorithms. Computer Science Proceedings 83, 1064–1069. doi: 10.1016/j.procs.2016.04.224.

the third Publication: 2017 by Aswathy and Jagannath. Digital histopathology image detection of breast cancer: current state and future prospects. [Online]. Inform. Med. Unlocked 8, 74–79. doi: 10.1016/j.imu.2016.11.001.

[4] Edited by Bayramoglu, Kannala, and Heikkilä (2016). "Deep learning for magnification independent breast cancer histopathology image classification," Paper presented at the 2016 ICPR annual conference. Publication: IEEE (Cancun, Mexico).

In 2013, Bengio, Courville, and Vincent published a paper. A review and fresh insights on representation learning was published in the IEEE Transactions on Pattern Analysis and Machine Intelligence journal, volume 35, pages 1798–1828 (doi: 10.1109/TPAMI.2013.50).

See, for example, Bergstra and Bengio (2012). Optimizing hyperparameters via a systematic search. Research in Machine Learning 13, 281-305.

[7] In 2013 (eds. by Borg, Lavesson, and Boeva), the authors were. Methods for Clustering Gene Expression Data and Their Comparison. At Aalborg, SCAI is located.

In 2008, Boyle and Levin published a paper. Publication: 2008 by the International Agency for Research on Cancer (IARC) Press, World Cancer Report.

[9] Author: Bradley, A. P., 1997. The process of evaluating machine learning algorithms using the area under the ROC curve. Volume 30, Issue 11, pages 1145–1159.

doi: 10.1016/S0031-3203(96)00142-2 [10] D. Colquhoun (2014). Looking at p-value misunderstandings and the false discovery rate. Scientific Reports, Series A, Volume 1, Issue 1, Page 140216. 10.1098, "Rsos.140216" [online].

(Ellis, 2010) [11]. The Definitive Resource for Understanding Effect Sizes in the Context of Meta-Analysis, Statistical Power, and Research Interpretation. Cambridge University Press: New York, NY.

[12] In a 2017 study, Esteva, Kuprel, Novoa, Ko, Swetter, Blau, and colleagues examined... Dermatologist-level classification of skin cancer utilizing deep neural networks. Publication: Nature 542, 115-118. Nature publication number: 21056

13 Filipczuk, P., Fevens, T., Krzyzak, A., &Monczak, R. (2013). Cytological pictures from small needle biopsies are the basis for computer-assisted breast cancer diagnosis. 32, 2169-2178. doi: 10.1109/TMI.2013.2275151. Published in the IEEE Transactions on Medical Imaging.

In 2014, George, Zayed, Roushdy, and Elbagoury published a paper. A cytology-based remote computer-assisted breast cancer detection and diagnostic system. 8(949)-964, 2013 (doi:10.1109/JSYST.2013.2279415), IEEE Systems Journal.

[15] In 2016, Gulshan et al. were joined by Peng, Coram, Stumpe, Wu, and Narayanaswamy. A deep learning method for diabetic retinopathy diagnosis in retinal fundus photographs: development and validation. doi: 10.1001/jama.2016.17216. JAMA 316, 2402-2410.